PhotoniX

RESEARCH Open Access

Electric field enhancement of coupled plasmonic nanostructures for optical amplification

Jun Hyun Kim[1], Ja Yeon Lee[2], Eung Soo Kim[3] and Myung Yung Jeong[4*]

*Correspondence:
myjeong@pusan.ac.kr

[1] Department of Cogno-mechatronics Engineering, Pusan National University, Busan 46241, Korea
[2] ESPn Medic, ESPn Medic cooperation, Busan 46241, Korea
[3] Department of Electronic & Robotics Engineering, Busan University of Foreign Studies, Busan 46234, Korea
[4] Department of Optics and Mechatronics Engineering, Pusan National University, Busan 46241, Korea

Abstract

Plasmonic effects that enhance electric fields and amplify optical signals are crucial for improving the resolution of optical imaging systems. In this paper, a metal-based plasmonic nanostructure (MPN) is designed to increase the resolution of an optical imaging system by amplifying a specific signal while producing a plasmonic effect via a dipole nanoantenna (DN) and grating nanostructure (GN), which couple the electric field to be focused at the center of the unit cell. We confirmed that the MPN enhances electric fields 15 times more than the DN and GN, enabling the acquisition of finely resolved optical signals. The experiments confirmed that compared with the initial laser intensity, the MPN, which was fabricated by nanoimprint lithography, enhanced the optical signal of the laser by 2.24 times. Moreover, when the MPN was applied in two optical imaging systems, an indistinguishable signal that was similar to noise in original was distinguished by amplifying the optical signal as 106 times in functional near-infrared spectroscopy(fNIRS), and a specific wavelength was enhanced in fluorescence image. Thus, the incorporation of this nanostructure increased the utility of the collected data and could enhance optical signals in optics, bioimaging, and biology applications.

Keywords: Plasmonic effect, Nanostructure, Nanoimprint lithography, Field enhancement, Amplifying optical intensity, Selective deposition fabrication

Introduction

In recent decades, micro/nanostructures based on plasmonic effects that amplify optical signals induced in plasmonic nanostructures, modulate optical signals, and enhance localized electric fields have attracted considerable attention, and plasmonic nanostructures that interact with light have been used to enhance image resolution, detect molecules, and change optical properties. Moreover, plasmonic nanostructures have been used in various fields, such as biology, imaging, medicine, and photonics, including surface-enhanced Raman spectroscopy (SERS) [1–3], surface-enhanced infrared absorption [4, 5], fluorescence imaging [6, 7], and nonlinear optics [8–15]. Metallic nanostructures with plasmonic resonance, in which free electrons oscillate in resonance with propagating light waves, have various characteristics depending on the size and shape of the structure and the type of

material [13, 14, 16]. For example, dipole antennas can transmit and receive radiofrequency radiation. At the resonant frequency, i.e., when the frequency of the incident radiation matches the natural vibration frequency of the material, the induced electric and magnetic fields are enhanced. At the macroscale, such resonance occurs when the dipole antenna structure has dimensions of $\lambda/2$, where λ is the wavelength of the incident radiation. However, at the nanoscale, the dimensions of the material at which resonance with radiation of wavelength λ occurs depend on the properties of the material itself. Thus, a dipole nanoantenna must be tuned to convert freely propagating radiation fields into localized energy [17–19]. Additionally, bowtie nanoantennas can enhance electric fields in nanogaps fabricated from two rectangular shapes using surface plasmon resonance (SPR). SPR involves electromagnetic (EM) waves that are generated by the free electrons in metals. The most effective phenomenon that occurs in plasmonic nanostructures is EM resonance, in which the free electrons in the metal layers oscillate at the same frequency as the incident radiation [20–22]. In this study, we designed a plasmonic nanodevice that amplifies optical signals to enhance the spatial resolution of optical imaging systems. The proposed plasmonic nanostructure was designed based on nanoantenna and grating nanostructure theory, and the structure can amplify specific optical signals 2.24 times based on SPR and the coupling of the electric field in each structure. Additionally, we observed an enhanced electric field by using atomic force microscopy (AFM). Moreover, when we applied a metal-based plasmonic nanostructure (MPN) in the imaging system, we detected an indistinguishable signal by amplifying the original signal 76 times, resulting in a clearer image.

Results and discussion

Design of a plasmonic nanostructure coupled with dipole and grating nanostructures

To enhance the image resolution, the optical signal must be amplified, and the noise must be removed. As shown in Fig. 1, we designed and synthesized a metal plasmonic nanostructure (MPN) using dipole nanoantenna (DN), bowtie nanostructure (BN), and grating nanostructure (GN) theories to determine the suitability of these nanostructures for amplifying optical signals in the near-infrared (NIR) range to enhance the image resolution. The nanostructure proposed in this paper was first simulated to confirm the enhancement and coupling of the electric field to amplify the optical signal of the image. The designed MPN has three components: a plasmonic part (PP), horizontal part (HP), and vertical part (VP). The PP enhances the electric field in the nanostructure. As previously mentioned, the plasmonic effect, which involves the free electrons in the metal oscillating in resonance with the incident light, enhances the electric field by resonance matching the vibration of the electrons and the incident light wave vector (k). Momentum matching can be achieved by various methods, such as prism-coupled SPR with a Kretschmann geometry via a subwavelength grating (which reduces the size and complexity of the Kretschmann geometry) [12, 17, 23–26]. In this method, the surface plasmon polariton (SPP) wave vectors must satisfy the plasmonic equation to ensure the coupling of the incident light photons and SPP wave vectors:

$$k_{SPP} = \frac{\omega}{c}\sin\theta_{\alpha} + n\frac{2\pi}{a}$$

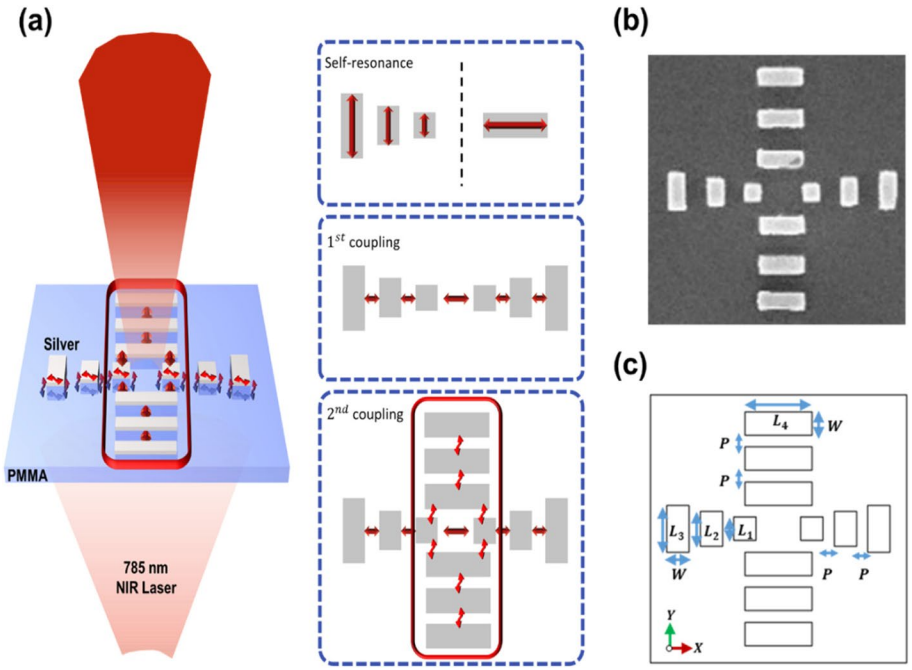

Fig. 1 **a** Schematic of a metal-based plasmonic nanostructure (MPN) for amplifying a specific optical signal. The MPN has three resonance parts to enhance the optical signal. **b** SEM image of the MPN, on which silver was deposited to obtain plasmonic effects. **c** Dimensions of the MPN for enhancing the electric field

where ω is the wave frequency of the incident light, c is the speed of light, θ_α is the incident light angle, n is an integer, and a is the grating period. Thus, the grating pitch is also a crucial parameter for achieving SPR, which results in the concentration of the electric field at the center of the nanostructure.

The VP was designed based on a DN to receive a specific wavelength. A DN enhances EM waves due to resonance in the structure for signal processing and radiation transmission. In contrast to antenna theory [18, 19, 27, 28], the shape and length of the DN need to be designed according to the wavelength because the refractive index differs depending on the structure (called the effective refractive index), similar to BNs and rectangular nanoantennas [13, 24, 25, 29–31].

The HP concentrates the electric field at the center of the nanostructure unit cell. In addition, the HP has a plasmonic effect on the surface. The HP was also designed based on the DN but with different lengths for each nanostructure to concentrate the electric field at the center of the unit cell, similar to the BN structure.

The finite element method (FEM) simulation tool was used to maximize the optical characteristics, such as the electric field enhancement, far-field gain of the MPN structure, and resonance of each structure. The key parameters for amplifying optical signals using the MPN are its dimensions (which determine the wavelength required to trigger the required resonance), the period of the structure, and the incident light angle required to generate a plasmonic surface.

Figure 1 shows that based on the DN characteristics, we optimized the length of the VP to 1177.25 nm, and its period was fixed at 196 nm, which is equal to λ/4, where λ is the excitation wavelength. The dimensions of the HP were fixed at 392.5 nm, 588.75 nm,

and 785 nm (corresponding to λ/2, 3λ/4, and λ, respectively, based on nanoantenna theory; in Fig. 1c, these dimensions are denoted as L_1, L_2, and L_3), and its period was fixed at 196 nm (λ/4; denoted as P in Fig. 1c).

As shown in Fig. 2, each nanostructure has a dipole momentum that occurs due to the oscillation of free electrons of silver atoms on the surface. However, the HP in the nanostructure has a small plasmonic effect, through which the electric field transmits the forward incident light, which concentrates the electric field according to grating theory [32], as shown in Fig. 2a, b. The VP receives a specific wavelength depending on its length and period, as shown in Fig. 2c. When both structures were combined, the electric field of the MPN was concentrated in the middle of the structure, confirming that such a dipole can be created on the surface of an Ag-based plasmonic nanostructure. Additionally, the electric field at the center of the structure was enhanced due to the plasmonic effects of each grating, as shown in Fig. 2.

For the 1177.25 nm VP, the generated electric field was confirmed to be 31.826 V/m, which was 15 times higher than that of the DN and GN structures, as shown in Fig. 3a. The magnitude of the electric field is also affected by the incident light angle due to the plasmonic effects mentioned above. When the plasmonic nanostructure resonates with the incident light, the extinction, scattering, and absorption cross-sections change.

Figure 3c, d, e confirm that the resonance of the MPN depends on the angle of incident light. As confirmed in Fig. 3c, when the angle of incident light to the MPN was 30°, the extinction cross-section was 1.33 $\times 10^{-11}$ m^2, whereas the extinction cross-sections of the GN, BN, and DN structures were 3.97 $\times 10^{-13}$ m^2 , 4.716 $\times 10^{-14}$ m^2, and 7.873 $\times 10^{-16}$ m^2, respectively. Thus, for an incident light angle of 30° (Fig. 3a, b), the electric

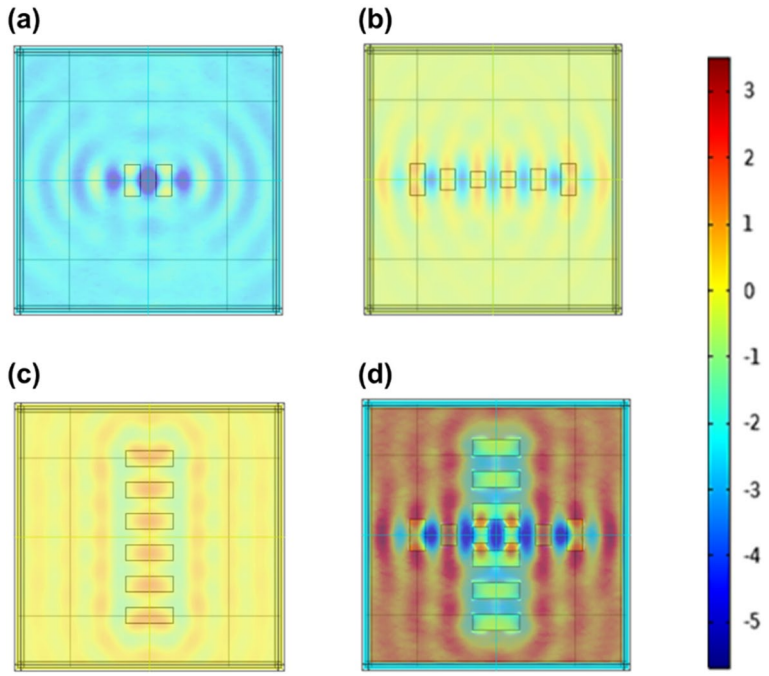

Fig. 2 DN, BN, GN, and MPN simulation data. **a** shows the DN results. **b** shows the BN results. **c** shows the GN results. **d** shows the MPN results. The proposed plasmonic nanoantenna enhances the electric field in the middle of the structure, and the electric field enhancement is 15 times greater than that of the DN and GN

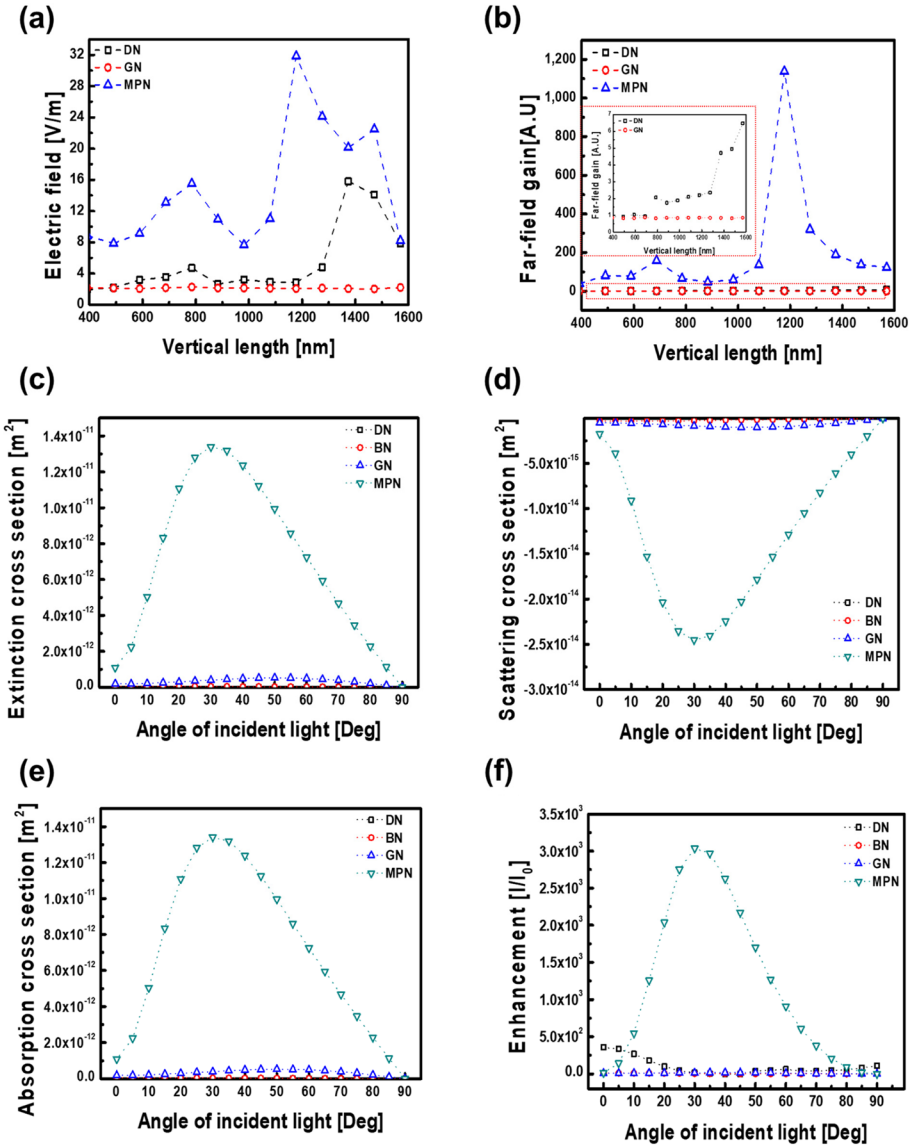

Fig. 3 MPN simulation data. **a** Simulation of the electric field in the output domain depending on the vertical lengths of the MPN, GN, and DN. **b** Simulation of the far-field gain depending on the vertical lengths of the MPN, GN, and DN. **c, d, e** Simulation of the extinction, scattering, and absorption cross-sections of the MPN, GN, and DN depending on the angle of incident light. **f** Graph of enhancement achieved with the MPN, GN, and DN

field and far-field gains were determined to be 31.826 V/m and 1137.8 V/m, indicating that the generated electric fields were 600 and 1100 times greater than those of the DN and GN, respectively.

The simulation data confirm that the proposed plasmonic nanoantenna can enhance the electric field concentrated in the middle of the nanostructure due to the coupling of the grating structure and dipole antenna, which both have plasmonic characteristics. Figure 3f shows the improvement in the optical intensity (I/I_0), which indicates that the plasmonic nanostructure enhances the optical signal by more than 226 times at a distance of 3 μm.

Selective deposition and fabrication

The MPN was fabricated by combining tape lithography and nanoimprint lithography (NIL). A schematic of each process step is shown in Supplementary 2. The Si material was fabricated using electron beam (e-beam) lithography. An e-beam resist (AR-P 6200, Allresist GmbH, Germany) was coated onto the Si wafer; subsequently, arrays of square nanopatterns were patterned using e-beam lithography (JBX-9300FS, JEOL Ltd., USA). The pattern width W was 392.5 nm; the period P was 196 nm; and the lengths L_1, L_2, L_3, and L_4 were 392.5 nm, 588.75 nm, 785 nm, and 1177.25 nm. The height was 230 nm, and the patterns were square arrays. Figure 4a, b show a scanning electron microscopy (SEM, SNE-3200 M, SEC, Korea) image of the fabricated Si stamp. Before the hybrid nanoimprinting process, the surface of the Si master was treated by dipping the Si master into a fluoric release agent solution (OPTOOL DSX, Daikin Industries Ltd., Japan, 147 µL and FC-3283, 3 M, USA, 50 g) for 10 min. This treatment decreased the surface energy of the Si mold, facilitating demolding during the nanoimprinting process to enable stronger van der Waals force-based bond formation between the Si mold and Ag atoms. After the surface treatment, the contact angle of the Si master was measured using a contact angle meter (Phoenix, SEO, Korea). The increase in the contact angle from 55.10° to 115.14° confirmed that the

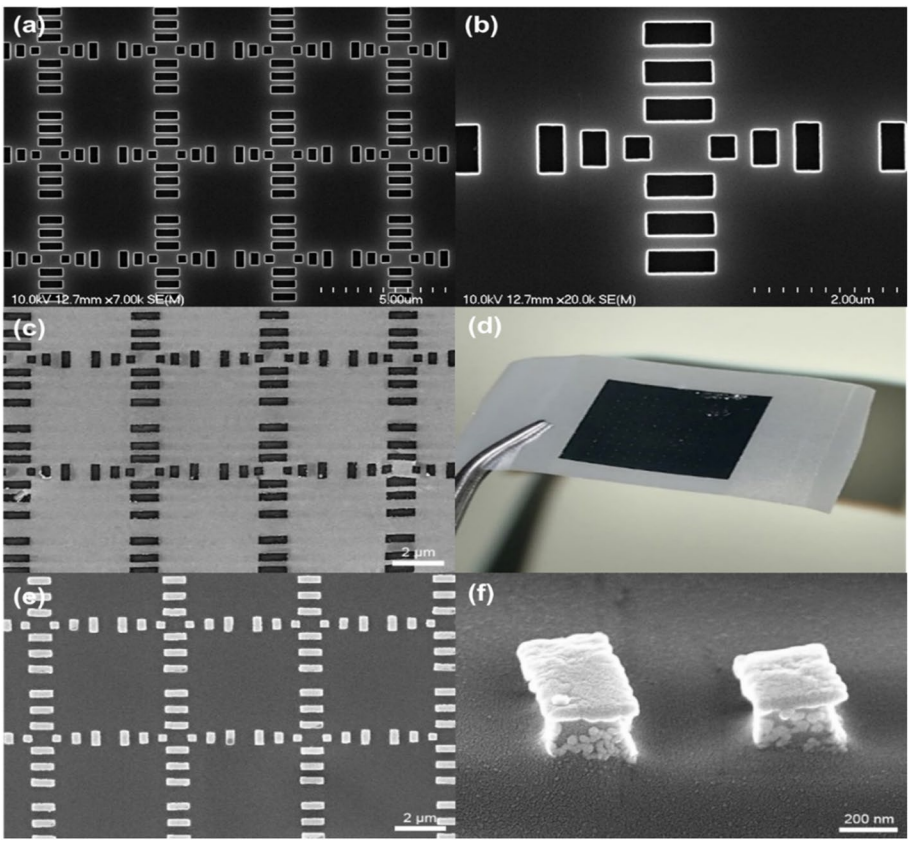

Fig. 4 **a, b** SEM image of the Si mold. **c** SEM image of adhesive tape. As shown in (**c, d**), Ag was peeled off the mold because it was required for selective deposition on the nanostructure. **e, f** SEM image of the final MPN. **e** shows Ag selectively deposited on the polymeric nanostructure

release agent was bonded to the surface of the Si master and that the surface treatment had been performed properly, as shown in Supplementary 3.

A 50-nm-thick Ag film (3–5 mm granules, 99.99%, Taewon Scientific Co., Ltd.) was deposited onto the Si master using an e-evaporator (MEP5000, SNTEK Co. Ltd., Korea). The deposition rate determines the roughness and (more importantly) grain size of the resulting thin metal film. As light scattering at the grain boundaries in metals has been reported to lead to losses, the deposition rate was varied from 1 to 20 Å/s. After metal deposition, adhesive tape (3 M; St. Paul, MN, USA) was used to remove the metal protruding from the surface of the Si master. The adhesion of the metal varied according to the substrate used: Ag showed poor adhesion with Si and was therefore easily transferred to the adhesive tape. Figure 4c, d show SEM images of the Ag nanopatterns stripped off the adhesive tape, confirming that the protruding Ag film was the only material removed by the adhesive tape.

A thermal NIL process (NIL-6, Obducat, Germany) was used to fabricate noble-metal plasmonic nanostructures. Prior to this process, a one-step procedure was performed to fabricate nanostructures on a polymethyl methacrylate (PMMA) substrate, and the Ag layer was transferred to this nanostructure. This process was conducted at 145 °C and a maximum pressure of 4 MPa over 300 s, with a demolding temperature of 75 °C.

Figure 4e, f show the final nanostructure fabricated using thermal imprint lithography. Figure 4f demonstrates that the silver was selectively transferred from the mold to the substrate according to the difference in surface energy. Fidelity analysis was conducted on the final structure. The ideal length was 1177.25 nm, where the length of the fabricated Si master was 1144.9 nm and that of the fabricated plasmonic nanostructure was 1130.2 nm. Accordingly, the fidelity was determined to be 2.43%, which was lower than the simulated tolerance value of 3.8%. This result confirms that the proposed hybrid imprint process is an effective and accurate method for fabricating MPNs.

Plasmonic effects of the nanostructures

To confirm that the MPN enhances the optical signal, a 785 nm laser was used with a laser–detector (fiber) distance of 3 cm, as shown in Supplementary 1. Figure 5 demonstrates that the light intensity is enhanced by using a plasmonic structure. Figure 5a shows that the plasmonic nanostructure amplifies the optical intensity depending on the incident light angle. In this graph, the input power passing through the collimator was 0.1791 mW. However, after the light passed through the plasmonic nanostructure, the power increased to 0.4022 mW at an incidence angle of 30°. We calculated the normalized intensity by comparing the reference intensity with the intensity after amplification by the plasmonic nanostructure. Compared with the original laser, the light intensity was 2.24 times higher after the laser passed through the plasmonic nanostructure. This increase occurred because light that would otherwise be scattered in the air and by the surface was concentrated in the middle of the nanostructure. When the difference between the orientation of the plasmonic nanostructure and the laser direction was 0°, the detected power decreased slightly. When the plasmonic effect occurred, which resulted in resonance with the incident light wave vector, the highest output power intensity was observed at an incident light angle of 30°. This result indicates that the EM

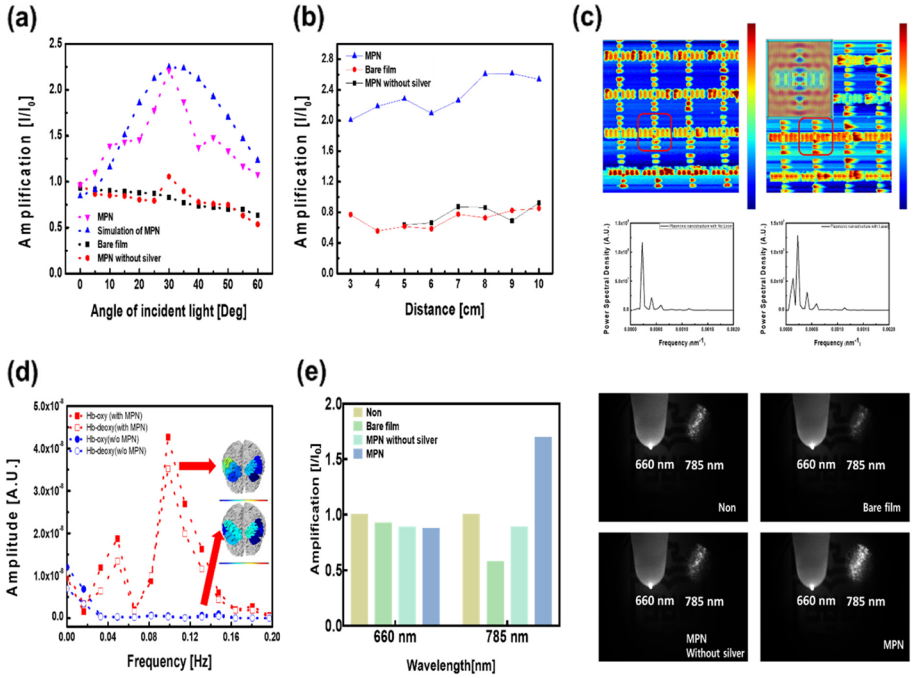

Fig. 5 Graph showing the dependence of the amplified optical signal on the distance, angle of incident light, and application. **a** shows that the plasmonic nanostructure amplifies the optical intensity when the plasmonic and incident light wave vectors are matched. When the angle of incident light is 30°, the plasmonic and incident light wave vectors are matched. **b** shows the amplification depending on the distance, demonstrating that the plasmonic nanostructure was more affected when the optical intensity was weak. **c** shows AFM data which without the laser(left) and with laser(right). **d** shows the amplitudes of oxyhemoglobin and deoxyhemoglobin for the plasmonic nanostructure, which were used as controls. This subfigure also shows the amplitudes of oxyhemoglobin and deoxyhemoglobin for the plasmonic nanostructure with detectors 1 and 2. Detector 2 applied the plasmonic nanostructure at 30°. also shows the fNIRS spectra, indicating that a higher intensity was obtained with the plasmonic nanostructure (right) than with the original structure (left). **e** shows the fluorescence image and amplification graph; the amplitude of the optical signal is 1.6 times higher than that of the original signal

wave from the incident light was reinforced on the surface of the MPN by the EM wave of the latter (comparing Figs. 3f and 5a).

Figure 5b shows the amplification of the signal intensity based on the distance between the source and the detector. This figure demonstrates that the plasmonic nanostructure enhances the optical signal at an incident light angle of 30°. We also confirmed that the lower the input power is, the greater the output power is enhanced. Comparing the MPN and the bare film (PMMA), the MPN amplifies the optical signal by up to 2.61 times when the distance is 9 cm because of the coupling and enhancement of the electric field in the unit cell. However, the amplification obtained by the bare film and the nanostructure without silver is less than 0.92 owing to the transmittance of ~ 90%.

Figure 5c shows atomic force microscopy (AFM) images and power spectral density (PSD) spectra of the MPN without and with a laser, which can provide insights into the amplification of the optical electric field by an external electric field. The AFM topography was characterized using cantilever tips in tapping mode. The AFM surface topography image without the laser is consistent with the SEM image, in which the film morphology features of the MPN and P are 230 nm and 193 nm, respectively. When the

laser beam is incident at 30° on the MPN structure, the height of the MPN structure increases to 280 nm. Moreover, the height difference of the MPN with the laser, which was detected using AFM cantilever tips, is comparable to the electric field difference in the simulation. This finding indicates that the atomic force interaction between the cantilever tips and the MPN structure was affected by the electric field difference, which was attributed to the incident laser. This atomic force interaction due to the electric field was quantified through PSD calculations as a series of fast Fourier transforms. The PSD spectra show periodic signals as peaks, which are functions of the frequency. Compared with the PSD results of the MPN structure without a laser, we observed a new peak at approximately 0.001 nm^{-1} in the PSD spectrum of the MPN structure with a laser, and the amplitude of the peak is comparable to that of other reference peaks. The new periodic signal was similar to the signal obtained with the structure, suggesting a high correlation between the laser incidence angle (control variable) and the MPN structure. The AFM data showed plasmonic effects and the coupling of the electric field in each structure, confirming that the electric field in the MPN was enhanced.

Figure 5d shows the enhanced focused NIR spectroscopy (fNIRS) spatial resolution for brain activation imaging due to the enhanced brain signal. fNIRS is a brain activation imaging system that observes changes in oxyhemoglobin and deoxyhemoglobin using NIR light, which can penetrate the brain like a banana shape. Because light passing through the brain is absorbed and scattered by many other cells including skull, melanin and water, the spatial resolution of fNIRS in the vertical direction can only be confirmed within about 1 cm [33]. The deep signal cannot distinguish with noise signal because of weak signal. Figure 5d shows the amplitudes of the signals of detectors 1 and 2 versus the frequency for a normal control experiment with brain activation (circle) and MPN experiment (square). The amplitudes of the oxyhemoglobin and deoxyhemoglobin signals are nearly the same at 1.19×10^{-8} and 6.9×10^{-9} at 0 Hz, respectively, in the normal control experiment and 1.07×10^{-8} and 9.55×10^{-9}, respectively, in the MPN experiment. However, at frequencies greater than 0.02 Hz, the signals that change in the brain but are not detected in the normal control experiment are higher than the control values of 5.6×10^{-10} and 3.32×10^{-10}. Brain activation can be detected because the signals are amplified by more than 76 and 106 times, respectively, to 4.26×10^{-8} and 3.52×10^{-8}. In Fig. 5d, the brain images show the brain activation region and the extent of brain activation, as indicated by the changes in oxyhemoglobin and deoxyhemoglobin. This confirmed the activation signal at a deeper level by amplifying the signal 76 and 106 times (red line) which could not confirm whether the signal was activated because the signal was weak by absorbed and scattered by many cells (blue line).

Figure 5e shows a fluorescence image indicating the enhancement of a specific wavelength. Compared with the fluorescence image at 660 nm, the laser signals at 785 nm were amplified by up to 1.6 times, whereas the amplitude of the fluorescence signal at 660 nm was decreased by 0.87. Thus, the MPN can enhance specific wavelength signals due to the dipole nanoantenna and plasmonic effect. To confirm resolution with optical signal, we measure the optical signal and fluorescence image from the IR card with symbol as shown Supplementary 4 and 5. Compared with bare film, MPN without silver and original signal, MPN amplified optical signal 1.6 times than original signal from the IR card and can detect distance of image accurately as 1.94 mm than bare film, MPN

without silver and original signal as 1.695 mm, 1.739 mm and 1.808 mm that exact length of image which we detect is 2 mm. And Supplementary 5 shows using MPN can detect weak signal which similar to noise. Due to plasmonic effect, the intensity of original signal as 68.75 which is similar with noise intensity amplified 1.6 time as 110 can distinguish with noise.

Conclusion

In summary, we demonstrated a new plasmonic nanostructure to amplify specific optical signals to enhance the resolution of optical imaging systems. This nanostructure was designed based on a grating nanostructure and a dipole nanoantenna. Moreover, the proposed nanostructure causes plasmonic effects and amplifies optical signals through resonance and electric field coupling between each structure while concentrating the electric fields. Our results show that the MPN can enhance signals at selected wavelengths by using a dipole antenna, and we observed a twofold increase in power compared with that predicted in simulations. The proposed structure was designed to receive a specific laser wavelength of 785 nm (typically used in optical imaging) and to not amplify light in the near field but integrate light in the far field. We first examined the effectiveness of the proposed plasmonic nanostructure using FEM simulations (COMSOL Multiphysics 5.6a) to determine the possible electric field, far-field gain, and current density generated using this nanostructure.

According to the simulations, the optimal vertical length for the structure was 1177 nm, with transverse lengths of 393 nm and 588 nm, which were applicable for a laser wavelength of 785 nm. For a structure with a height of 180 nm, an Ag layer with a height of 50 nm, and an incident laser angle of 30°, the electric field was observed to be concentrated in the center and reached a value of 31.826 V/m, which was more than 15 times greater than that obtained with the DN and GN. Moreover, a far-field gain of 1137.8 was obtained.

Based on these design data, we fabricated a structure using thermal imprint lithography, followed by Ag deposition onto a specific nanostructure. Consequently, we observed that the intensity in the MPN was approximately three times higher than that in a bare film. Moreover, the intensity in the MPN was 2.24 times higher than the original laser intensity because the laser photons were concentrated in the middle of the structure and had a high directivity toward the detector. A device with these characteristics is superior to existing fNIRS systems. Our device identifies optical brain signals that cannot be distinguished by existing systems by increasing the signal-to-noise ratio and amplifying the optical signal by 106 times compared with the original system. Furthermore, amplifying the specific optical signal enhances the spatial resolution of the fluorescence optical imaging system. Therefore, our device can be used to enhance the diagnosis, staging, and investigation of treatments for neurological ailments, such as Alzheimer's disease, dementia, and stroke, for which there are currently few therapeutic options.

Methods/experimental

The MPN simulations were performed using the FEM method (COMSOL Multiphysics 5.6a), which is standard in the literature [17, 21, 28, 34–36]. To confirm the enhancement of the electric field in the unit cell, we set the computing size as a 5.795

by 5.795 μm surface that contains the plasmonic nanostructure, and the height was set at 3 μm in air. To set a nanostructure array condition for the metal-based material and confirm only the plasmonic effect of the nanostructure, each side of the nanostructure had a perfectly matched layer (PML) with a thickness of 150 nm to minimize reflections at the boundaries, and all the sides of the unit cell were treated with a periodic condition in front of the PML. The accuracy of the calculation was increased using a mesh set equal to the $\lambda/6$, namely, 130 nm, and the parameters of the COMSOL simulation were set as follows: number of elements: 290221, minimum element mesh size of the plasmonic nanostructures: 1.89×10^{-8} nm and maximum element mesh size: 140 nm. The incident light was transmitted through the bottom of the structure. The power of the incident light (I_0) was set to 10 mW/m^2, and a detector was placed on the upper side of the structure. The structure used in the simulation consisted of air, the substrate, the nanostructure, and silver layers. Air layers were placed at the bottom and top of the structure in the matching experiment. The nanostructure and substrate were composed of PMMA, and the refractive index varied depending on the wavelength. Different refractive indices were set for the silver layer depending on the wavelength based on the Lorentz–Drude model.

Optical characterization of the as-prepared MPN array was performed using an optical spectrum analyzer (OSA, Anritsu Co., MS9710C, Japan). Light from a 785 nm laser was irradiated through a fiber (@ 0.22 NA) onto the sample. To match the reference, the 785 nm laser source was divided by 1-by-2 multimode couplers, which divide the power according to the ratio 1:9, with a core size of 105 μm and a numerical aperture (NA) of 0.22 (TM105R2F1A, Thorlabs, USA). As shown in Supplementary Fig. 1, a fiber conveying 10% of the light was connected to the OSA and used to verify the power and wavelength of the reference. Subsequently, a fiber conveying 90% of the light was connected to a collimator (F240FC-780, Thorlabs, USA) to increase the spot size. Then, a laser was connected to the collimator, which directed the laser to the plasmonic nanostructure. All the experimental setups, including the composite sample holder, laser holder, and detector, could be moved to enable the correct alignment of all sections. The alignment between the detector and the laser was confirmed using a multifunction optical meter (Newport Co., 1936-R) and an OSA. The MPN array was placed between the laser and the detector, which were separated by a distance of 3 cm (Supplementary 1). The OSA can detect wavelengths in the range of 600–1750 nm with a bandwidth of 0.05 nm at intensities ranging from − 85 to 10 dB. As described above, the plasmonic effect enhances the electric field when the incident light and plasmonic wave vectors are matched. To enable this matching, the noble-metal plasmonic nanostructure was placed on a 360° rotation stage; the laser power was modulated in the range of 0–450 mW; and the power meter detection range was 7–20 kJ. The proposed plasmonic nanostructure was studied by tilting the nanostructure film and changing the laser intensity. Brain activation was confirmed using a static phantom similar to the brain refractive index, absorption, and scattering using fNIRS (NIRScout X, NIRx, CANADA) to determine the amplification of the brain signals. Brain activation was confirmed using eight sources and four detectors that could diagnose the cortex. To confirm the plasmonic effect of the nanostructure in

enhancing the brain signal, the plasmonic nanostructure was placed in detector 1 at 0° or detector 2 at 30°, and the other detector was used as a control.

Abbreviations

SERS	Surface enhanced Raman spectroscopy
SPR	Surface plasmon resonance
EM	Electromagnetic
DN	Dipole nanoantenna
BN	Bowtie nanostructure
GN	Grating nanostructure
MPN	Metal-based plasmonic nanostructure
PP	Plasmonic part
HP	Horizontal part
VP	Vertical part
FEM	Finite element method
SEM	Scanning electron microscopy
NIL	Nanoimprint lithography
PMMA	Polymethyl methacrylate
AFM	Atomic force microscopy
PSD	Power spectral density
fNIRS	Functional near-infrared spectroscopy
PML	Perfectly matched layer
OSA	Optical spectrum analyzer

Supplementary Information

The online version contains supplementary material available at https://doi.org/10.1186/s43074-023-00086-4.

Additional file 1: Supplementary 1. Schematic of the experimental and optical characteristics of the metal-based plasmonic nanostructure. **Supplementary 2.** The entire procedure for fabricating a metal plasmonic nanostructure. **Supplementary 3.** Contact angle for changing surface energy. **Supplementary 4.** Experimental optical characteristics of the metal-based plasmonic nanostructure for enhancing the resolution. **Supplementary 5.** Experimental of the metal-based plasmonic nanostructure for enhancing the resolution by fluorescence image.

Acknowledgments
Not applicable.

Authors' contributions
J. H. Kim designed and simulated the newly proposed plasmonic nanostructure. He collected the simulation data, prepared the figures, and wrote the manuscript. In addition, he performed optical and fNIRS experiments on the plasmonic nanostructures. J. Y. Lee developed the fabrication method and fabricated the plasmonic nanostructures. M. Y. Jeong and E. S. Kim conceived and supervised the project. All the authors contributed to the critical reading and writing of the manuscript. All the authors have read and agreed to the published version of the manuscript.

Funding
This study was supported by a National Research Foundation of Korea (NRF) grant funded by the Korean government (MSIT) (No. 2022R1A2B5B01002377).and Following are results of a study on the "Leaders in Industry-university Cooperation 3.0" Project, supported by the Ministry of Education and National Research Foundation of Korea.

Availability of data and materials
The datasets and figures used and analyzed in the present study are available from the corresponding author upon reasonable request.

Declarations

Ethics approval and consent to participate
Not applicable.

Consent for publication
Not applicable.

Competing interests
The authors have no conflicts of interest to declare.

Received: 23 August 2022 Revised: 28 January 2023 Accepted: 1 February 2023
Published online: 08 February 2023

References

1. Shanthil M, Thomas R, Swathi RS, George TK. Ag@SiO2 Core-Shell nanostructures: distance-dependent Plasmon coupling and SERS investigation. J Phys Chem Lett. 2012;3(11):1459–64.
2. Lee SY, Hung L, Lang GS, Cornett JE, Mayergoyz ID, Rabin O. Dispersion in the SERS enhancement with silver nanocube dimers. ACS Nano. 2010;4(10):5763–72.
3. Mahigir A, Chang TW, Behnam A, Liu GL, Gartia MR, Veronis G. Plasmonic nanohole array for enhancing the SERS signal of a single layer of graphene in water. Sci Rep. 2017;7(1):14044.
4. Bagheri S, Weber K, Gissibl T, Weiss T, Neubrech F, Giessen H. Fabrication of square-centimeter Plasmonic Nanoantenna arrays by femtosecond direct laser writing lithography: effects of collective excitations on SEIRA enhancement. ACS Photonics. 2015;2(6):779–86.
5. Chae J, Lahiri B, Centrone A. Engineering near-field SEIRA enhancements in Plasmonic resonators. ACS Photonics. 2016;3(1):87–95.
6. Cui X, Tawa K, Hori H, Nishii J. Tailored Plasmonic gratings for enhanced fluorescence detection and microscopic imaging. Adv Funct Mater. 2010;20(4):546–53.
7. Kim K, Yajima J, Oh Y, Lee W, Oowada S, Nishizaka T, et al. Nanoscale localization sampling based on nano-antenna arrays for super-resolution imaging of fluorescent monomers on sliding microtubules. Small. 2012;8(6):892–900 786.
8. Genevet P, Capasso F, Aieta F, Khorasaninejad M, Devlin R. Recent advances in planar optics: from plasmonic to dielectric metasurfaces. Optica. 2017;4(1):139–52.
9. High AA, Devlin RC, Dibos A, Polking M, Wild DS, Perczel J, et al. Visible-frequency hyperbolic metasurface. Nature. 2015;522(7555):192–6.
10. Kildishev AV, Boltasseva A, Shalaev VM. Planar photonics with metasurfaces. Science. 2013;339(6125):1232009.
11. Liu Z, Wang Q, Xie Y, Zhu Y. High-efficiency control of transmitted light with a three-layered plasmonic metasurface. J Phys D Appl Phys. 2016;49(47):475101.
12. Minovich AE, Miroshnichenko AE, Bykov AY, Murzina TV, Neshev DN, Kivshar YS. Functional and nonlinear optical metasurfaces. Laser Photonics Rev. 2015;9(2):195–213.
13. Schnell M, García-Etxarri A, Huber AJ, Crozier K, Aizpurua J, Hillenbrand R. Controlling the near-field oscillations of loaded plasmonic nanoantennas. Nat Photonics. 2009;3(5):287–91.
14. Schuller JA, Barnard ES, Cai W, Jun YC, White JS, Brongersma ML. Plasmonics for extreme light concentration and manipulation. Nat Mater. 2010;9(3):193–204.
15. Ahmadivand A, Sinha R, Pala N. Resonance coupling in plasmonic nanomatryoshka homo- and heterodimers. AIP Adv. 2016;6(6):065102.
16. Cubukcu E, Kort EA, Crozier KB, Capasso F. Plasmonic laser antenna. Appl Phys Lett. 2006;89(9):093120.
17. Novotny L, van Hulst N. Antennas for light. Nat Photonics. 2011;5(2):83–90.
18. Muhlschlegel P, Eisler HJ, Martin OJ, Hecht B, Pohl DW. Resonant optical antennas. Science. 2005;308(5728):1607–9.
19. Novotny L. Effective wavelength scaling for optical antennas. Phys Rev Lett. 2007;98(26):266802.
20. Crozier KB, Sundaramurthy A, Kino GS, Quate CF. Optical antennas: resonators for local field enhancement. J Appl Phys. 2003;94(7):4632–42.
21. Grober RD, Schoelkopf RJ, Prober DE. Optical antenna: towards a unity efficiency near-field optical probe. Appl Phys Lett. 1997;70(11):1354–6.
22. Guo H, Meyrath TP, Zentgraf T, Liu N, Fu L, Schweizer H, et al. Optical resonances of bowtie slot antennas and their geometry and material dependence. Opt Express. 2008;16(11):7756–66.
23. Abb M, Wang Y, de Groot CH, Muskens OL. Hotspot-mediated ultrafast nonlinear control of multifrequency plasmonic nanoantennas. Nat Commun. 2014;5:4869.
24. Berkovitch N, Ginzburg P, Orenstein M. Nano-plasmonic antennas in the near infrared regime. J Phys Condens Matter. 2012;24(7):073202.
25. Ishi T, Fujikata J, Makita K, Baba T, Ohashi K. Si Nano-photodiode with a surface Plasmon antenna. Jpn J Appl Phys. 2005;44(12):L364–L6.
26. Mironov EG, Khaleque A, Liu L, Maksymov IS, Hattori HT. Enhancing weak optical signals using a Plasmonic Yagi—Uda Nanoantenna Array. IEEE Photon Technol Lett. 2014;26(22):2236–9.
27. Hofmann HF, Kosako T, Kadoya Y. Design parameters for a nano-optical Yagi–Uda antenna. New J Phys. 2007;9(7):217.
28. Kosako T, Kadoya Y, Hofmann HF. Directional control of light by a nano-optical Yagi–Uda antenna. Nat Photonics. 2010;4(5):312–5.
29. Biagioni P, Huang JS, Hecht B. Nanoantennas for visible and infrared radiation. Rep Prog Phys. 2012;75(2):024402.
30. Cao L, Park JS, Fan P, Clemens B, Brongersma ML. Resonant germanium nanoantenna photodetectors. Nano Lett. 2010;10(4):1229–33.
31. Tahir AA, Schulz SA, De Leon I, Boyd RW. Design principles for wave plate metasurfaces using plasmonic L-shaped nanoantennas. J Optics. 2017;19(3):035001.
32. Gupta N, Dhawan A. Bowtie nanoantenna driven by a Yagi-Uda nanoantenna: a device for plasmon-enhanced light matter interactions. OSA. Continuum. 2021;4(11):2970–9.
33. Quaresima V, Ferrari M. Functional near-infrared spectroscopy (fNIRS) for assessing cerebral cortex function during human behavior in natural/social situations: a concise review. Organ Res Methods. 2016;22(1):46–68.
34. Bohn BJ, Schnell M, Kats MA, Aieta F, Hillenbrand R, Capasso F. Near-field imaging of phased Array Metasurfaces. Nano Lett. 2015;15(6):3851–8.
35. Li J, Fattal D, Li Z. Plasmonic optical antennas on dielectric gratings with high field enhancement for surface enhanced Raman spectroscopy. Appl Phys Lett. 2009;94(26):263114.
36. Zu S, Bao Y, Fang Z. Planar plasmonic chiral nanostructures. Nanoscale. 2016;8(7):3900–5.

Publisher's Note